scientific reports

Check for updates

OPEN

Improvement of the optical cavity-based biosensor's limit of detection using optimal 3-aminopropyltriethoxysilane process

Marzhan Sypabekova[1,3], Jenna Kleiss[1], Aidan Hagemann[1], Sophia Schuemann[1], Riley Wills[1], Bernd Zechmann[2] & Seunghyun Kim[1]✉

Optical resonator-based biosensors are important for advancing medical diagnostics and environmental monitoring due to their high sensitivity and label-free detection capabilities. In this study, we present a systematic comparison of three 3-aminopropyltriethoxysilane (APTES) functionalization methods - ethanol-based, methanol-based, and vapor-phase - on an Optical Cavity-based Biosensor (OCB) designed to detect streptavidin. The APTES process is an important first step for surface functionalization to form a linker to immobilize receptor molecules on the sensor surface. Our aim was to identify the deposition conditions that yield a uniform APTES layer, with an enhanced bioreceptor immobilization and improved sensor performance. By using a differential detection approach using two laser diodes at 808 nm and 880 nm, we achieved real-time intensity measurements in the OCB that enabled sensitive detection of target analyte. Among the three APTES methods tested, the methanol-based protocol (0.095% APTES) led to a significantly improved limit of detection (LOD) of 27 ng/mL, a threefold improvement over our previous results. Detailed atomic force microscopy (AFM), contact angle, and dose-response analyses confirmed the high quality of the monolayer formed under optimal conditions, emphasizing the importance of solvent choice and controlled deposition parameters for obtaining stable functional layers. These findings emphasize how the improved APTES functionalization directly enhances the sensitivity and reliability of our OCB system, offering a robust and adaptable approach for real-time, label-free detection in diverse biosensing applications.

Optical resonator-based biosensors, a subset of optical biosensors, utilize the principles of light confinement and interference within an optical cavity for the detection of biological analytes with high sensitivity. An optical cavity functions as a transducer by converting changes in its geometry or material - which alter resonance parameters - into variations in light intensity[1]. These biosensors are highly valued in medical diagnostics and environmental monitoring for their rapid, label-free detection capabilities. The most common types are Whispering Gallery Mode (WGM) resonator and Fabry-Perot Interferometer (FPI)[2]. WGM biosensors are based on ring or spherical-shaped structures to detect minute changes in refractive index (RI), temperature, pressure, and mechanical constraints around them[3,4]. FPI biosensors typically use two reflective surfaces to detect the biological interaction within them with a high sensitivity[5]. Recent research has highlighted several specific types of FPI biosensors, such as optical fiber-based FPIs, where the optical cavity is either integrated at the tip or within complex structures inside the fiber[6,7] and optical cavity-based FPIs that incorporate simple or advanced microfabricated structures within the cavity with two reflecting mirrors[8–10].

Advancements in optical resonator-based biosensor developments have demonstrated their capability to detect biomarkers at low concentrations and identify single molecules, making them as a frontier technology for pushing the boundaries of sensing[11–13]. While the potential for single-molecule detection positions these devices

[1]Department of Electrical and Computer Engineering, Baylor University, Waco, TX, USA. [2]The Center for Microscopy and Imaging, Baylor University, Waco, TX, USA. [3]Present address: Department of Bioengineering, Civil Engineering and Environmental Engineering, Florida Gulf Coast University, Fort Myers, FL, USA. ✉email: Seunghyun_Kim@baylor.edu

at the cutting edge of research tools, it also brings into question their practicality for everyday use. Important factors such as ease of use and reproducibility often do not receive enough emphasis, raising concerns about the feasibility of these technologies for reliable, targeted detection in practical settings[3]. Challenges like delicate integration and inconsistent reproducibility also still need to be addressed. Developing simpler integration techniques and enhancing reliability are essential steps to exploiting their full potential for widespread application, emphasizing the ongoing need for improvement in making these tools practically useful across various fields.

We have developed an Optical Cavity-based Biosensor (OCB) system utilizing a simple Optical Cavity Structure (OCS) based on an FPI[8,14–17]. The OCS is created by an SU8 pattern between two partially reflective silver layers defined by a simple photolithography process. The SU8 pattern also serves as a microfluidic channel to allow the sample fluid to flow through the OCS. When the collimated light wave propagates through the OCS, it experiences multiple beam interference, producing a characteristic transmission spectrum with resonant peaks. This resonance enables the detection of minute changes within the cavity, making the OCB a potent tool for label-free and highly sensitive detection. The binding of target analytes on immobilized receptor molecules within the OCS leads to shifts in the resonance transmission spectrum due to changes in the local RI. Instead of using expensive optical equipment to detect the resonance shift, our approach detects intensity changes using low-cost components like laser diodes and a charge-coupled device (CCD) or complementary metal oxide semiconductor (CMOS) camera while enhancing the sensitivity by employing a differential detection method[15]. Our results demonstrated the OCB's ability to detect C-reactive protein (CRP) at a limit of detection (LOD) of 377 pM and streptavidin at an LOD of 1.35 nM without amplification[8]. We have also optimized the detection capabilities by fine-tuning the reflectance of the surfaces and the differential detection approach[18].

The work presented here advances our previous findings by systematically optimizing and comparing different 3-aminopropyltriethoxysilane (APTES) functionalization protocols, leading to a significantly improved LOD that highlights the extended scope of this study. The APTES deposition method affects the quality of the receptor molecule functionalization therefore we attempted three different APTES deposition methods and found the optimal method that gives the best sensitivity for streptavidin detection. Among various target analytes, streptavidin stands out as a model protein due to its exceptionally high binding affinity and specificity for biotin[19]. This well-characterized interaction serves as a reliable benchmark in biosensor development, facilitating the validation of the sensor's performance. Moreover, the biotin-streptavidin system is widely used in clinical diagnostics, drug discovery, and environmental assays, making the improved detection of streptavidin directly relevant to a broad range of practical applications[20]. Although numerous approaches for APTES functionalization are available, our study goes beyond standard protocols by systematically comparing three distinct deposition methods: ethanol-based, methanol-based, and vapor-phase, under identical laboratory conditions. This side-by-side evaluation isolates the effect of each approach on sensor performance, providing a direct, quantitative assessment of how solvent and process variables impact the formation of a stable APTES monolayer. By refining these deposition parameters, we achieved a significantly improved LOD for our OCB platform, showing the tangible benefits of methodical silanization optimization.

Materials and methods

Materials

Soda lime glass (100 and 76.2 mm) substrates were obtained from UniversityWafer Inc., South Boston, MA, USA, and AZ photoresist (1518) and developer (300 MIF) were obtained from Integrated Micro Materials, Argyle, TX, USA. Spin-on-glass (IC1-200, SOG) was purchased from Futurrex Inc., Franklin, NJ, USA, and SU8 photoresist (SU8-2010) and SU8 developer were purchased from Kayaku Advanced Materials, Inc., Westborough, MA, USA, UV glue (NOA 86 H) was purchased from Norland Products Inc., Jamesburg, NJ, silver etchant (type TFS) was purchased from Transense Company Inc., Danvers, MA, USA. 2-propanol (IPA) and acetone (99%), were purchased from Thermo Fisher, Waltham, MA, USA. Bovine serum albumin (BSA), Streptavidin, and (3-Aminopropyl)triethoxysilane (APTES) were purchased from Sigma, St. Louis, MO, USA, Methanol from VWR, Radnor, PA, USA, Ethanol from Electron Microscopy Sciences, Hatfield, PA, USA, 99.99% pure silver target (2 inch diameter, 0.125 inch thick) from Kurt J. Lesker, Jefferson Hills, PA, USA, sulfo-NHS biotin from Thermo Scientific, Rockford, IL, USA.

Laser diodes (A pin code, Ø5.6 mm, 10 mW) at wavelengths 880 and 808 nm, 50:50 nonpolarizing beam splitter cube (BS014), antireflection (AR)-coated neutral density filter (NE550B-B), broadband dielectric mirror (BB1-E03), and corresponding mounts for each component (KM100T, CM1-4ER, FMP05, H45) were obtained from Thorlabs Inc., Newton, MA, USA. A charge-coupled device (CCD) camera (CM3-U3-13S2M-CS) was obtained from Point Grey Research Inc., Wilsonville, OR, USA and syringe pump was obtained from Cole Parmer, Vernon Hills, IL, USA. All aqueous solutions and rinsing steps were done using deionized (DI) water.

Simulations

The FIMMWAVE/FIMMPROP (Photon Design, Oxford, UK) software was used for all simulation results presented in this paper. We employed the fixed index model to simulate the efficiency changes of two different selected wavelengths upon the immobilization of target molecules. In the fixed index model, the number of the target molecules is approximated as the thickness of a layer with a fixed RI. We used 1.45 for the RI of the sensing layer, which has been widely used for various biomolecules.

Sample fabrication

Two low-cost soda lime glass substrates, each 550 µm thick and 76.2 mm in diameter, were utilized to construct the OCS's top (drilled substrate) and bottom (plain substrate) parts. The sample fabrication procedure was adapted from [5] with some modifications. Initially, a partially reflective silver layer (20 nm thick) was sputter-

deposited onto both substrates using an Ar flow of 60 sccm and a 100-W DC power setting (CRC, Torr LLC, New Windsor, NY, USA). For patterning the silver layer on the drilled substrate, AZ photoresist was spin-coated using a spin coater (WS-650-23, Laurel Technologies, Johnstown, PA, USA), followed by baking at 100 °C for 1 min on a hot plate. The substrate was then exposed to UV light using a mask aligner (OAI, Hybralign 500, Milpitas, CA, USA) for 60 s at an intensity of 5.7 mW/cm^2. The patterned photoresist was developed in AZ developer for 1 min, rinsed with DI water, and dried with N_2. The exposed silver areas were etched by immersing the substrate in a silver etchant for 15 s, followed by DI water rinsing and N_2 drying. Subsequently, the SOG layer was spin-coated at 850 rpm and cured on the drilled substrate at 130 °C for 4 min, followed by 95 °C for another 4 min. The SOG layer on the plain substrate was similarly processed but cured at 95 °C for 1 min, followed by 200 °C for 1 min. SU-8 2010 was then spin-coated on the plain substrate, soft-baked at 95 °C for 2 minutes, UV exposed for 90 s, and post-exposure baked at 95 °C for 3 min. After cooling for 1 min, the substrate was developed in SU-8 developer for 2 minutes, rinsed with IPA, dried with N_2, and baked at 200 °C for 10 min. To further protect the silver layer and facilitate silanization for biodetection, the drilled substrate was radio frequency (RF) sputter-coated with silicone dioxide (SiO_2) at 20 sccm and 100 W for 10 min (CRC, Torr LLC, New Windsor, NY, USA). Finally, oxygen plasma treatment was applied for 5 min to activate the surface for APTES functionalization by increasing the number of available hydroxyl (-OH) groups. After APTES functionalization and sNHS biotin attachment, both drilled and plain substrates were bonded together using UV glue. Spin-coated UV glue on the 100-mm glass "transfer" substrate was transferred onto the SU8 pattern on the plain substrate. The plain and the drilled substrates were immediately aligned and brought together using an in-house stamping/bonding stage. The sample was then cured under the mask aligner for 10 min at 5.7 mW/cm^2. The inlet and outlet ports were then attached to the top surface of the drilled substrate using double-sided tape (3 M 468MP) for the fluid in/out. Both inlet and outlet ports were made of acrylic cut using a laser cutter (Glowforge basic, Glowforge Inc., Seattle, WA, USA). The inlet port has an inner diameter (ID) of 2.5 mm and an outer diameter (OD) of 8 mm, while the outlet port has an ID of 1.37 mm and OD of 8 mm. A fluid was injected into the inlet port by pipetting, while a syringe pump in withdraw mode was used to flow the fluid from the inlet to the outlet through a Tygon tubing (OD 1.37 mm) attached to the outlet port.

Surface functionalization

The APTES deposition was carried out using three distinct methods to evaluate their effectiveness in preparing surfaces for biosensor applications. First, the ethanol-based method involved immersing the oxygen plasma-treated sample in 20 ml of a 5% (v/v) APTES solution in absolute ethanol. The container was shaken at 40 rpm (TYZD-IIII, Jiangsu Tenlin Instrument Co., China) at room temperature during the incubation period, followed by rinsing with ethanol, drying under N_2, and the final baking step. Second, for the methanol-based method, a stock solution of 50% methanol, 47.5% APTES, and 2.5% DI water was aged for at least one hour at 4 °C. At the time of the APTES process, the stock solution was diluted 1:500 in methanol and the samples were incubated in the solution followed by rinsing, drying, and baking steps. Lastly, vapor-phase deposition involved placing the sample in a desiccator with 0.5 mL of 99% APTES on a hot plate at 90 °C for 24 h. After the deposition, the substrate was ultrasonically washed in DI water, followed by a baking step.

Sulfo-NHS-biotin (sNHS-biotin) was freshly dissolved in DI water at a concentration of 5 mg/mL immediately prior to each use to ensure activity. For functionalizing the sensing area on the drilled substrate, 10 µL of this solution was precisely applied using a micropipette. The substrate was then incubated for 1 h in a humidity box, allowing the biotin to covalently bond to the surface through amide linkages, thereby ensuring stable attachment. Simultaneously, other areas were blocked using 1% bovine serum albumin (BSA) for 30 min to prevent nonspecific adsorption. This prepared surface was then utilized for the subsequent streptavidin detection experiments. Additionally, 500 µL of 1% BSA was applied as a blocking agent to the plain substrate with the SU-8 pattern for 30 min, further minimizing any nonspecific binding of streptavidin.

Testing setup

A schematic and real image of the detection setup for the OCS samples is shown in Fig. 1a and b. Laser diode drivers powered by a 5-V power supply employed a basic current-regulation circuit that maintained a stable operating current of 50 and 30 mA for the 808 nm and 880 nm diodes, respectively. Beams from two laser diodes were collimated, combined by a 50:50 beam splitter, and blocked for one-second intervals by an Arduino-controlled beam blocker such that they could be imaged sequentially. A neutral filter was placed in the beam's path for each laser diode to attenuate the intensities and avoid saturation. A mirror directed the beams toward the OCS sample, i.e. into a microfluidic channel sensing area. The microfluidic channel was connected to a syringe pump operating in withdraw mode at a flow rate of 1 µL/min, ensuring a controlled sample flow across the sensing region. Eventually, a low-cost CCD camera was used to collect the images of the OCS with both laser diodes.

The collected CCD images are then used to calculate the average intensities of both laser diodes in a designated data processing region (DPR) and display them in real-time. The DPR was defined as a circular region in the middle of the microfluidic channel with a diameter of 188 µm (equivalent to 50 pixels). Data acquisition from the CCD images and the calculation of differential values were conducted using IgorPro software, whereas data analysis and graphical display were managed through OriginPro. All measurements were carried out in triplicate, and the mean value of replicates, standard deviations, and standard errors from the mean were used to report the results.

STV detection

The microfluidic channel, with its biotin-functionalized sensing area, was thoroughly rinsed, filled with DI water, and left for at least 3 h to allow for signal stabilization prior to the detection experiments. After that, the

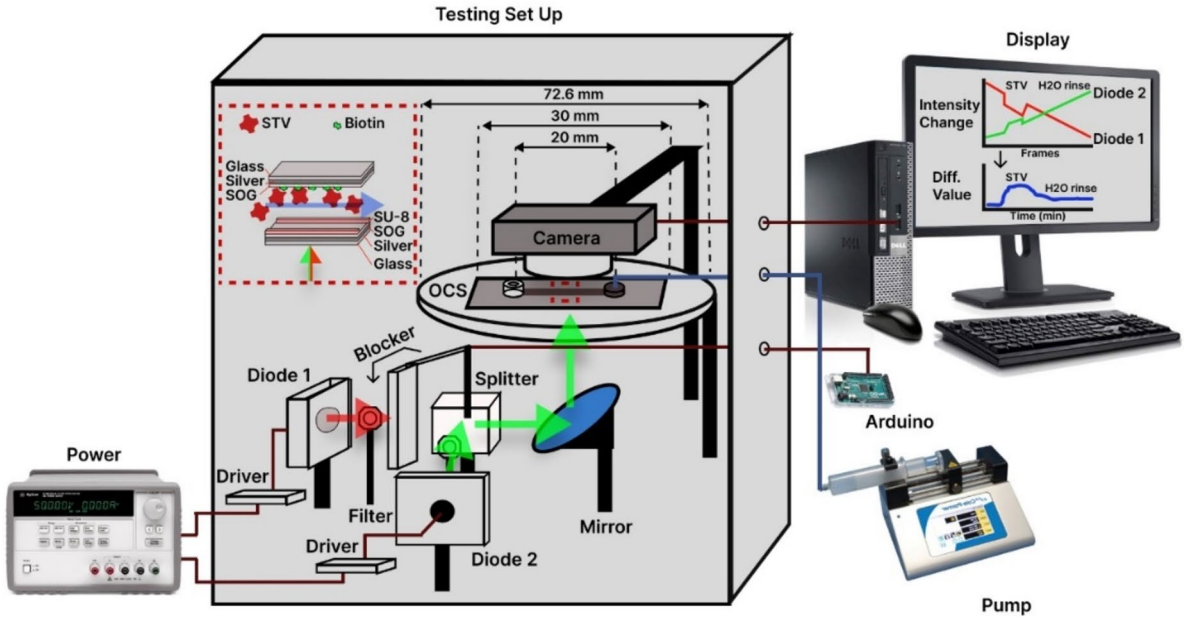

a

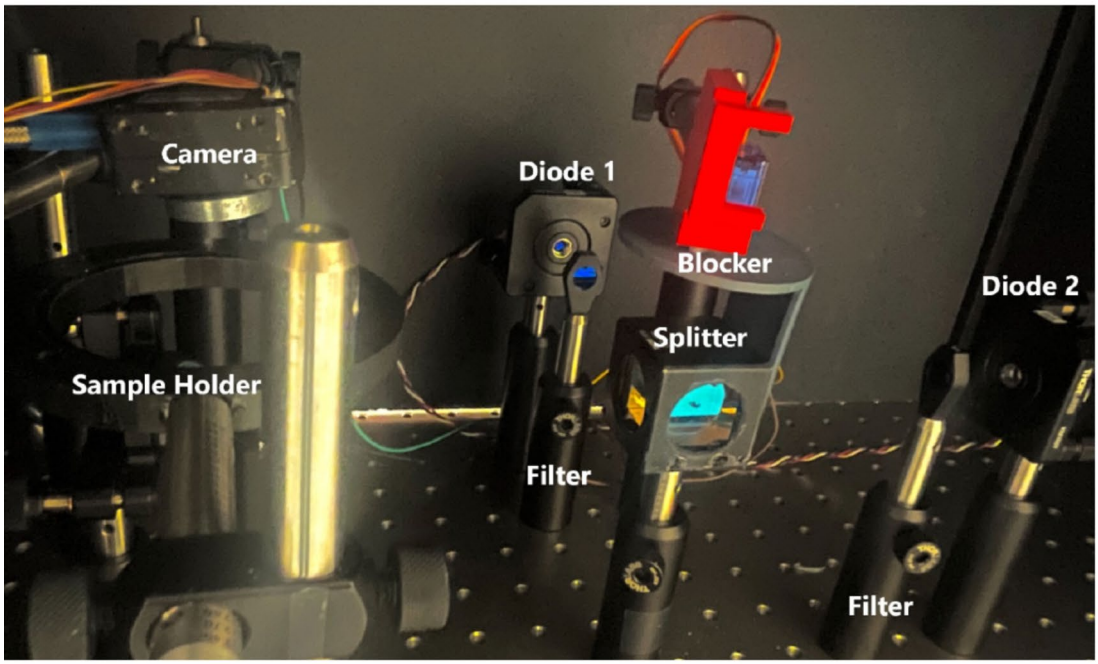

b

Fig. 1. (**a**) Schematics and (**b**) real image of the experimental set up.

sample was placed on a sample holder under the camera, and the outlet tubing was connected to the syringe pump. Initially, DI water was introduced in the sensing region for 2 min at a rate of 1 µL/min to establish a stable baseline. This was followed by the injection of streptavidin (STV) solution, which was allowed to interact with the biotinylated surface for 10 min at specified concentrations. Finally, the sensor surface was rinsed with DI water to remove any unbound STV molecules. Each concentration was tested three times using three functionally independent sensors. The intensities of both laser diodes were monitored in real-time during the entire experiment.

The surface morphology study and contact angle measurements

Surface morphology was analyzed using an Atomic Force Microscope (AFM), specifically the Dimension Icon model (Bruker, Germany), which achieves resolutions of less than 0.1 nm in the Z-axis and less than 1 nm in the X and Y axes. The microscope operated in ScanAsyst-Air mode, where the peak force was maintained as low as 10 pN through a feedback loop. Surface morphologies were assessed using a ScanAsyst-Air probe (Bruker, Germany) with a nominal spring constant of 0.4 N/m, a resonant frequency of 70 kHz, and a tip radius of 2 nm. All measurements were conducted at room temperature. The Gwyddion analysis software was utilized for visualizing the images and measuring the root-mean-square (RMS) roughness.

An in-house built optical angle setup was used for contact angle measurement. Samples were placed on the stage, and a 10 µL drop of DI water was dispensed. The wetting of the surface was then captured using a MU 900color CMOS camera (Amscope Irvine, CA) mounted on a stereomicroscope. The contact angle was measured using an on-screen protractor.

Results and discussion

OCS and OCB design

The OCS used for this investigation was initially designed by simulations. Figure 2 shows the schematic of the OCS, including two partially reflective silver layers, two SOG layers, an SU8 channel, and UV glue and the simulations results. The changes in efficiencies of 808 nm and 880 nm wavelengths for the sensing layer thickness from 0 to 10 nm on one of the SOG surfaces were calculated. The OCS is carefully engineered so their efficiencies change in opposite directions as the sensing layer thickness increases. Then, we employed a differential detection method using the equation shown below to maximize the sensitivity. The differential value (η) is determined by[8,18]

$$\eta = \frac{I_1 - I_{10}}{I_{10}} - \frac{I_2 - I_{20}}{I_{20}},$$

where I_1 and I_2 are the intensities (or efficiencies for simulations) of 880 nm and 808 nm, respectively, and I_{10} and I_{20} represent the initial intensities for I_1 and I_2, respectively.

Although single-wavelength intensity measurements can be prone to drift and noise, our dual-wavelength differential approach significantly reduces common-mode fluctuations. By carefully engineering each optical component of the OCS such as two partially reflective silver layers, precise SOG thickness, and an SU8 microchannel, the OCB maximizes localized hotspots for increased sensitivity. In addition, by capturing the intensity of two different laser diodes (808 nm and 880 nm) in quick succession and calculating the differential value, we isolate the signal change attributed to the sensing layer from broader environmental influences or power instabilities. This method preserves the benefits of a simple, cost-effective intensity-based setup, while delivering high precision comparable to more complex resonance-shift detection techniques. The differential metric between the two laser diodes amplifies signal changes caused by analyte binding, effectively suppressing background noise and system fluctuations.

The silver thickness is fixed to 20 nm to be consistent with our previous works. Based on the resonance characteristics of the OCS at this silver thickness, we determined the cavity width (i.e., the distance between two silver surfaces) to be 13.79 µm. Within the OCS, light waves experience multiple beam interference because

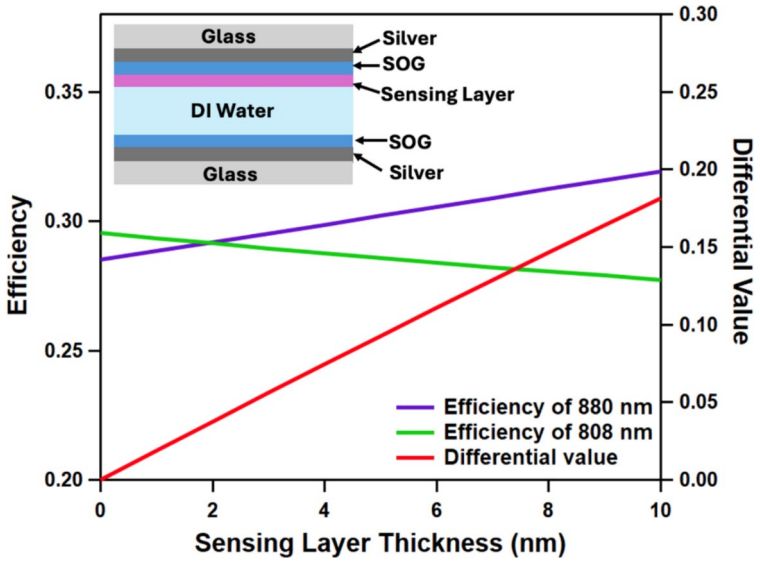

Fig. 2. Schematic of the OCS and simulation results. The calculated differential value change (0.182) is greater than the individual efficiency changes of 808 nm (-0.018) and 880 nm (0.034) for the sensing layer thickness change of 10 nm.

of two partially reflective silver layers, creating an interference field pattern. Due to the interference pattern, electromagnetic field strength is stronger at certain locations, forming optical hotspots, within the OCS. At the hotspots, the sensitivity is maximized upon the local RI change. Therefore, we simulated the OCS with different SOG thicknesses and chose an SOG thickness of 465 nm based on the possible hotspots.

The initial efficiencies of 808 nm and 880 nm were 0.296 and 0.285, respectively. For a sensing layer thickness change from 0 to 10 nm, the efficiency of 808 nm decreased to 0.277 (efficiency change: -0.019) and that of 880 nm increased to 0.319 (efficiency change: 0.034), while the differential value changed from 0 to 0.182. The results show a significant response enhancement with the differential detection method (Fig. 2).

Although the present OCB setup appears more suitable for a laboratory environment, its reliance on low-cost, readily available components (e.g., laser diodes, CCD camera) makes it amenable to miniaturization and automation. By integrating these optical elements and electronic drivers into compact housing and implementing user-friendly software for data processing, the OCB platform could be adapted for point-of-care testing or on-site environmental monitoring.

Surface roughness

The SOG layer not only allows the molecular binding to occur at the selected hotspot location to maximize the sensitivity, but it also plays an important role in (1) protecting the underlying silver (Ag) layer from oxidation and other environmental factors that could potentially degrade the sensor's performance over time and (2) reducing the surface roughness. A smooth surface could potentially improve the sensitivity and specificity of the OCB through a well-organized silane layer from APTES treatment, which then allows outward-facing amine groups, facilitating efficient biotin conjugation via NHS ester chemistry.

Figure 3 shows AFM images and surface roughness measurement results from fabricated samples. The root mean square (RMS) roughness values for the glass substrate, sputter-deposited silver layer, and SOG surface are 0.263 ± 0.0018 nm, 3.239 ± 0.047 nm, and 0.658 ± 0.0022 nm, respectively. The results demonstrate the SOG layer reduces the surface roughness close to that of the glass substrate itself.

Comparing three different APTES deposition methods

APTES, a silane coupling agent, forms a self-assembled monolayer on oxide substrates, presenting amine groups that readily react with biomolecules or additional cross-linking agents. It is primarily used for surfaces that contain hydroxyl (-OH) groups, such as silicon dioxide or metal oxides. Its silane functional group reacts with these -OH sites to form stable siloxane (Si–O–Si) bonds, while the terminal amine (-NH2) moiety is available to couple further with biomolecules (e.g., via crosslinkers or direct conjugation). Consequently, this process is not directly compatible with surfaces like gold, where thiol (-SH) chemistry is typically preferred. Nonetheless, if the gold surface is first coated with a thin oxide layer or another suitable intermediate film bearing -OH groups, an APTES-based modification could be performed.

The APTES process is important for surface functionalization because it affects the quality of the bioreceptor layer where the analytes bind. For optimal biosensor performance, an APTES monolayer is preferred over multilayers because thick silane layers are unstable and can be washed away during incubation or rinsing steps, resulting in reduced sensor performance[21–23]. In this study, we evaluated three different APTES immobilization

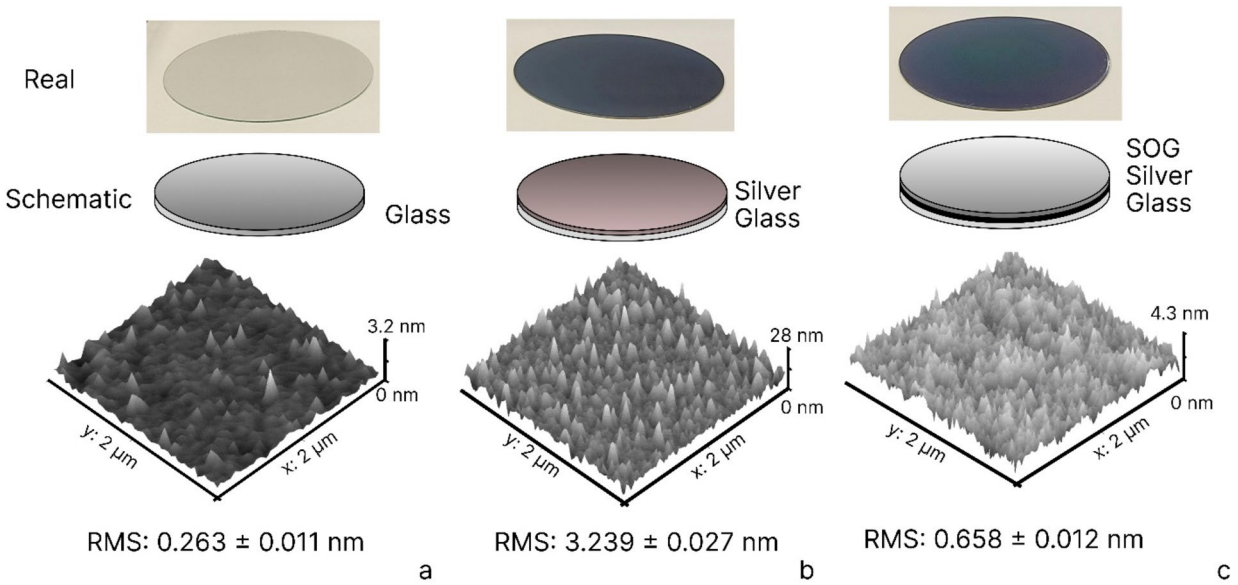

Fig. 3. Surface Roughness of Different Substrate Configurations. Real Image: Shows a real photograph of the substrate. Schematic: Depicts the schematic representation of the substrate. AFM Image: Displays the AFM analysis of the substrate, with a root mean square (RMS) roughness of (**a**) glass substrate, (**b**) sputter-deposited silver surface, and (**c**) SOG surface.

methods that are widely used: 5% APTES in ethanol solution, 0.095% APTES in methanol solution, and vapor phase deposition. Our goal was to identify the best APTES functionalization technique for our OCB out of these three and demonstrate an improved LOD of the OCB.

Figure 4a illustrates the steps involved in the surface functionalization process using APTES, performed only for the drilled substrate. The process begins with the preparation of the silicon dioxide surface, which is then treated with oxygen plasma to activate the surface with hydroxyl groups. This is followed by the application of APTES, forming a self-assembled layer. Subsequently, the surface is biotinylated using sNHS-Biotin for the detection of streptavidin. The detailed protocols for each APTES functionalization method are illustrated in Fig. 4b. For the method with 5% APTES in ethanol (ethanol-based method), the surface was treated with a 20-minute immersion at room temperature followed by baking at 120 °C for 20 min. The method with 0.095% APTES in methanol (methanol-based method) involved immersion of the drilled substrate in the solution for 20 min, followed by a baking process at 110 °C for 30 min. For the vapor phase deposition method (vapor-phase method), the drilled substrate is exposed to APTES vapor for 24 h and then baked at 110 °C for 10 min after sonication. After APTES functionalization and sNHS-Biotin immobilization, each sensor was allowed to interact with 1.25 µg/mL streptavidin after the initial baseline in DI water at a 1 µL/min flow rate. The sensor

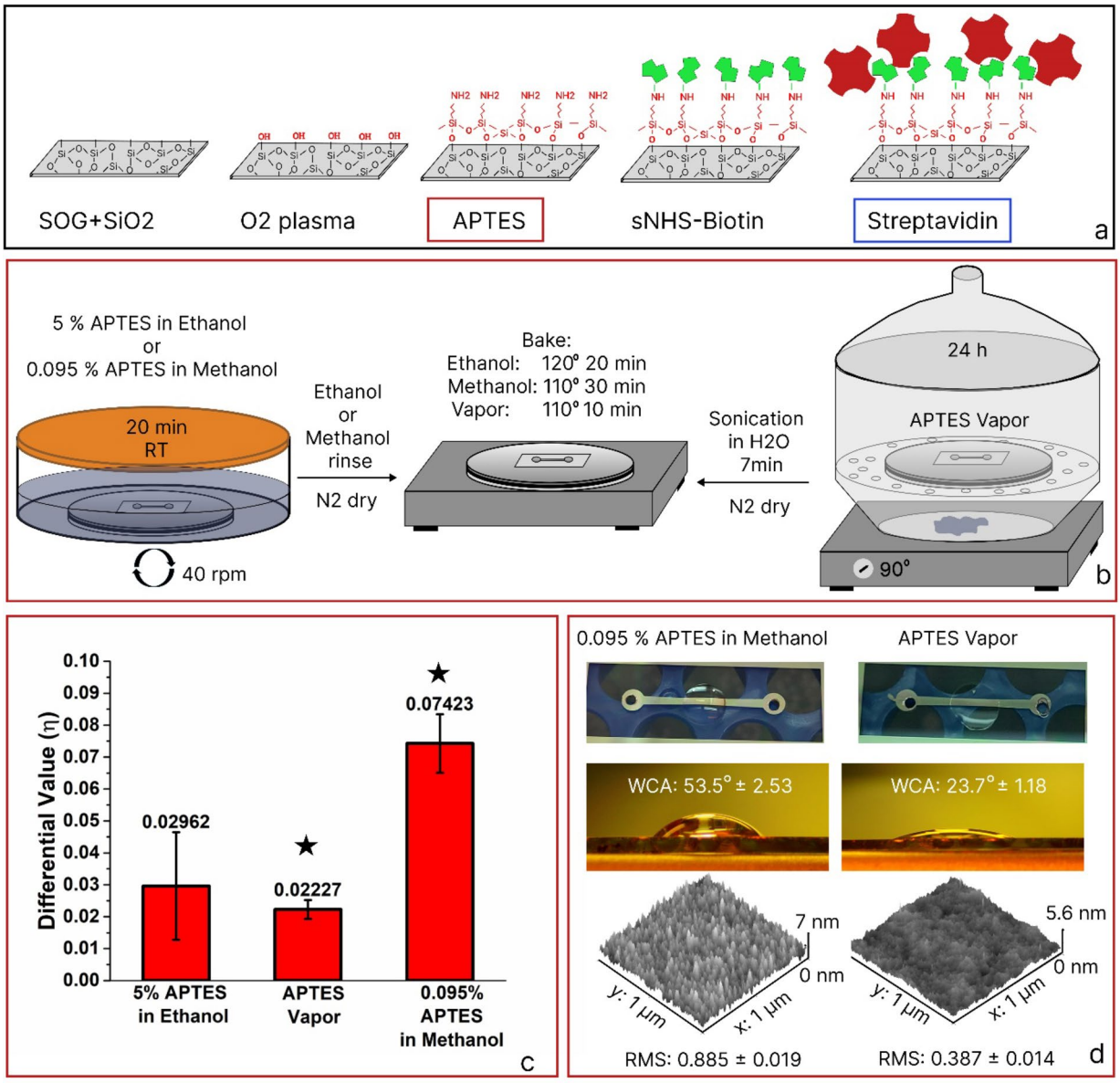

Fig. 4. (**a**) Schematic of surface functionalization process. (**b**) Detailed protocols for APTES functionalization. (**c**) Triplicate measurement results, showing the average differential values with an error bar (+/- standard deviation). Asterisks indicate the APTES methods that showed less variability and were further investigated for WCA and RMS roughness. (**d**) WCA and AFM measurement results for surfaces treated with 0.095% APTES in methanol and APTES vapor.

surface was rinsed with DI water, and the corresponding differential value change was obtained. The last 2 min of data were used to report the results.

The triplicate test results with 1.25 μg/mL streptavidin for all three APTES processes are shown in Fig. 4c. The methanol-based method yielded the largest differential value change (0.07423 ± 0.00916). The vapor-phase method and the ethanol-based method resulted in differential value changes of 0.022227 ± 0.00296 and 0.02962 ± 0.01683, respectively. To understand the cause of this response difference between different APTES processes, we compared the surface wettability and surface roughness using WCA and AFM measurements for the methanol-based and vapor-phase methods, which showed less sample-to-sample variation with smaller error bars compared to the ethanol-based method. The top images of Fig. 4d show the 10 μL sNHS-biotin droplet on the APTES-treated sensing area after incubation. The sample surface with the methanol-based method exhibited a WCA of 53.5° ± 2.53, whereas the surface with the vapor-phase method showed a significantly lower WCA of 23.7° ± 1.18. AFM analysis showed that the surface with the methanol-based method had an RMS roughness of 0.885 ± 0.019 nm while that of the vapor-phase method was 0.387 ± 0.014 nm. For an APTES monolayer formation, it has been reported that, on average, the surface after APTES treatment becomes more hydrophobic, with a WCA range of 40–65 degrees and surface roughness of 0.7–0.8 nm[21,24]. These results indicate that the best and most stable responses were achieved with the methanol-based method because it effectively forms a monolayer of APTES and, therefore, the most stable and effective biotin layer for streptavidin detection was created. The superior performance observed with the methanol-based APTES method likely comes from the distinct chemical kinetics of alkoxysilane hydrolysis and subsequent siloxane network formation in methanol. Methanol's higher polarity and lower boiling point can accelerate hydrolysis, facilitating a more uniform monolayer of APTES. This promotes stronger covalent linkage between the silanol groups on the substrate and the APTES molecules, leading to a highly stable, single-layer coverage. In contrast, ethanol has a slightly lower polarity and higher boiling point, potentially slowing down hydrolysis and inducing multilayer or patchy deposition. The vapor-phase approach may suffer from uneven condensation rates, particularly where local humidity and temperature can vary, limiting its capacity to achieve a dense and robust layer. Consequently, the methanol-based method may not only ensured an optimal balance of hydrolysis and condensation but also provided a homogeneous environment for forming a consistent monolayer of APTES.

STV detection

Using the methanol-based method, we performed triplicate tests to demonstrate an improved LOD of the OCB for streptavidin detection. From the samples fabricated for this experiment, the average Ag and SOG thicknesses were measured to be 20 nm and 464.85 nm, respectively, using an ellipsometer (M2000, J.A. Wollam, Lincoln, NE, USA). The SU-8 2010 and UV glue layers averaged 11.9 μm and 0.75 μm in thickness, as determined by a profilometer (D-500, KLA Tencor, Milpitas, CA, USA). For each measurement, DI water was first introduced through the microfluidic channel and the baseline data were collected. Then, different concentrations of 10 μL of streptavidin were introduced at a flow rate of about 1 μL/min. Finally, the channel was rinsed with DI water, and the change in the differential value due to the binding of streptavidin was measured by averaging differential values after rinse. Figure 5a shows the results for five different concentrations and the negative control (0 ng/mL). The average differential value changes were as follows: 0.070 ± 0.00014 at 2.5 μg/mL, 0.075 ± 0.01164 at 1.25 μg/mL, 0.050 ± 0.01164 at 625 ng/mL, 0.032 ± 0.01286 at 313 ng/mL, and 0.011 ± 0.00126 at 78 ng/mL. The differential value for the negative control result was 0.00018. These results indicate a specific binding of streptavidin to the biotin-functionalized surface and clear dose-response relationship, with higher streptavidin concentrations leading to greater differential value changes. At lower streptavidin concentrations (78–625 ng/mL), the results exhibited a linear differential value response, while the signal plateaued at higher concentrations (1.25–2.5 μg/mL) due to surface saturation for available receptor sites. This saturation likely contributes to the increased variability and larger error bars observed at the higher concentrations. As the binding sites approach saturation, minor variations in the surface coverage or the molecular orientation of the bound molecules may result in disproportionately large changes in the measured differential value, thereby increasing the observed variability. APTES primarily served as a platform for covalently attaching sulfo-NHS-biotin, which in turn provides the high-affinity biotin-streptavidin interaction. To minimize nonspecific adsorption, we included a 1% BSA blocking step. To further validate the sensor's performance, additional studies are needed to assess its specificity and potential cross-reactivity with similar proteins, ensuring its robustness for broader biosensing applications.

The LOD for our OCB with the methanol-based method was determined by the sensor response exceeding the 3σ threshold (0.00296), utilizing an analytical approach to evaluate the assay's sensitivity at low concentrations. For the precise calculation of the LOD, particular attention was given to the lower range of concentrations (up to 625 ng/mL), analyzed using linear regression to better approximate the initial response curve as shown in Fig. 5b. The calculated LOD was 27 ng/mL, corresponding to 450 pM of streptavidin, indicating a 3 times improvement in sensitivity compared to the previous work[8]. As a secondary method to validate the immobilized streptavidin on the functionalized sensing area, we performed an AFM scan, as shown in Fig. 6a. Figure 6b shows the topographical surface of the streptavidin-covered area after the streptavidin incubation. The topographical surface showed a grain-like structure with an average height of 4.3 ± 1.706 nm, which is in agreement with the dimension of streptavidin in previously published work[25,26].

The results show how an optimized APTES process substantially enhances sensor performance, specifically by forming a stable monolayer that yielded a threefold improvement in the LOD for streptavidin. Our approach demonstrated that slight variations in deposition conditions (e.g., solvent choice, deposition method) can profoundly affect the APTES layer - ranging from a uniform monolayer to a thick, irregular coating. Such variation critically influences both sensor stability and detection sensitivity. Our systematic comparison between APTES deposition protocols revealed that each lab must carefully optimize its own process rather than assuming

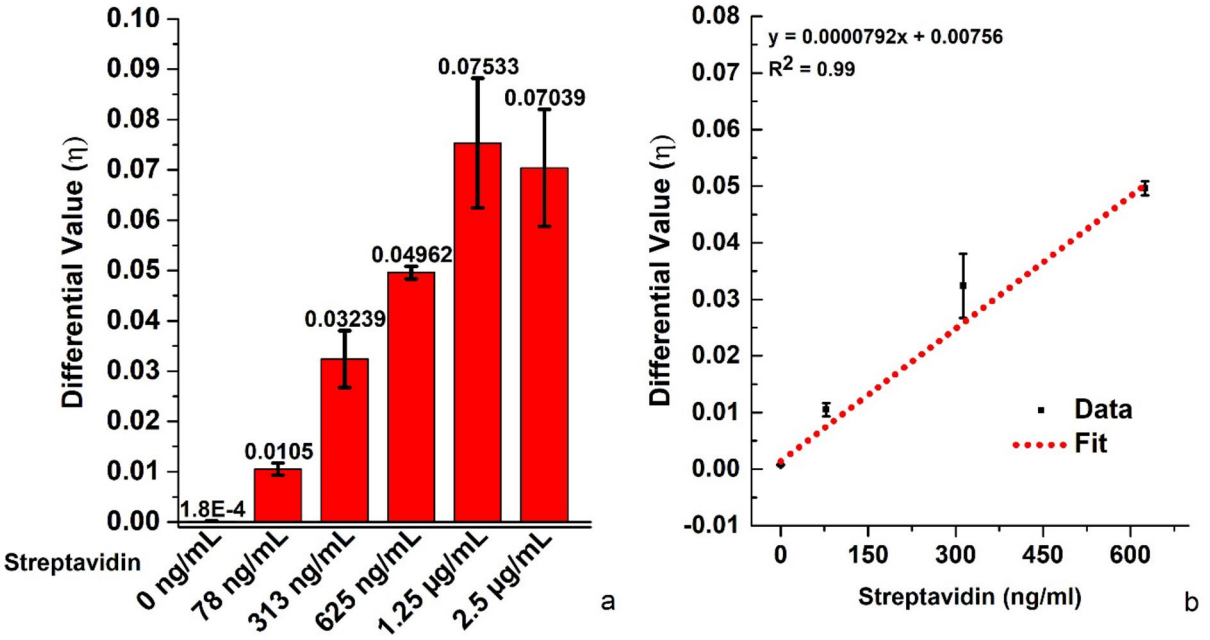

Fig. 5. (**a**) Average differential values for five distinct streptavidin concentrations and negative control samples. (**b**) Linear regression analysis of the differential values for streptavidin detection at lower concentrations (78–625 ng/mL). The plot shows a dose-response relationship, with the linear fit (dotted red line, $R^2 = 0.99$) between streptavidin concentration and the differential value, indicating the sensor's sensitivity in this range.

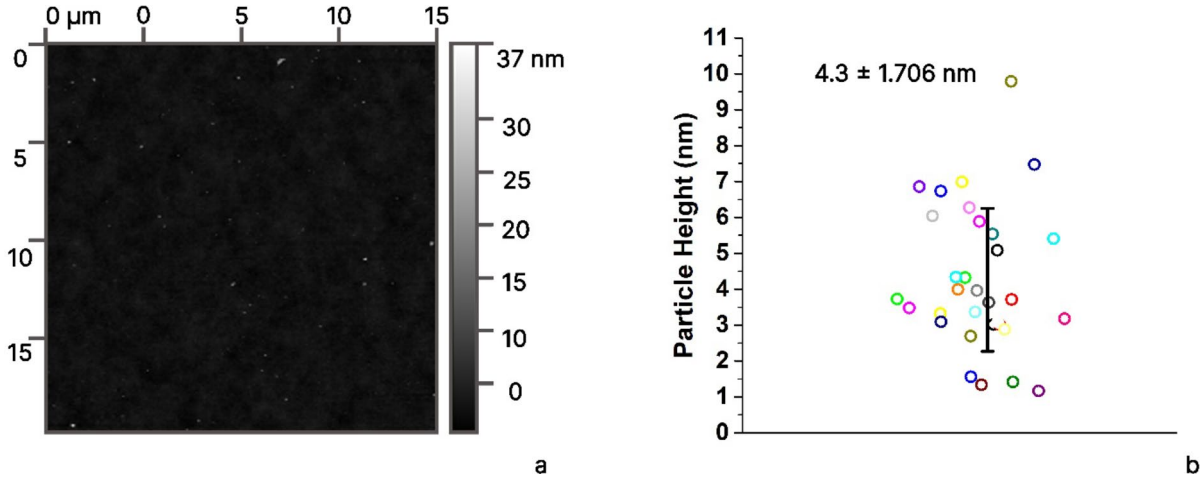

Fig. 6. (**a**) AFM image of the sensing area after the streptavidin incubation. (**b**) Particle size distribution and the mean size of the particle height.

a universal protocol would work[12]. Consequently, direct comparisons of LOD values across different studies may be misleading unless the APTES functionalization conditions are meticulously standardized.

Overall, these findings show the importance of tailoring APTES deposition to each experimental setup for consistent biosensor performance. By confirming that a methanol-based method offers a significantly improved LOD, we demonstrated that careful control of silane hydrolysis and condensation steps benefits not only our OCB design but can guide broader applications in high-sensitivity, label-free biosensing. Nevertheless, while the methanol-based method yielded reliable monolayer formation and enhanced sensitivity, more detailed studies are needed to assess the sensor surface's long-term performance. Although monolayer films generally exhibit better stability compared to multilayered structures, investigating potential degradation over time and under varying environmental conditions is extremely important. Furthermore, in moving toward large-scale manufacturing, rigorous process control and validation, particularly for humidity and temperature will be necessary to maintain consistent monolayer formation. Employing techniques that characterize chemical

composition and shelf life will ultimately provide a more comprehensive understanding of surface longevity and reliability in real-world biosensing applications.

Conclusion

In this study, we compared three different APTES methods in terms of the responsivity (differential value change) of the OCB for high-concentration streptavidin detection. The results showed that 0.095% APTES in methanol was superior to the other ethanol-based and vapor-phase methods. Based on the WCA and RMS roughness analysis, we concluded this result is due to a more stable and functional monolayer created using the methanol-based method, which further improved biosensor performance and reproducibility.

We then successfully demonstrated an improved LOD of the OCB for streptavidin detection with the methanol-based method. The triplicate test results show the LOD is 27 ng/mL (450 pM) for streptavidin, which is 3 times more sensitive than our previous work. The AFM particle size analysis confirmed the presence of streptavidin on the biotin-functionalized sensing area.

Taken together, these enhancements in the OCB's detection sensitivity have direct real-world applications. In clinical diagnostics, early identification of low-abundance biomarkers is important for timely intervention in diseases. Environmental monitoring also stands to gain from detecting trace contaminants such as heavy metals or pathogens, enabling preventive measures well before they escalate.

Note that we acknowledge the importance of specificity in biosensing applications. Streptavidin was chosen as a model molecule due to its strong affinity rather than as a target biomarker for a specific disease, making the identification of potential interfering molecules less straightforward. Also, it is important to note that while a novel differential detection method was employed to enhance the sensitivity, this approach does not eliminate the influence of non-specific binding or protein cross-reactivity. Instead, differential detection is expected to help mitigate common external noise, improving measurement reliability.

Moving forward, future work will focus on demonstrating the OCB with the methanol-based APTES functionalization technique to detect specific disease biomarkers, experimentally assessing both LOD and specificity in comparison to other proteins. Additionally, experimental validation will be conducted to evaluate the impact of non-specific binding and cross-reactivity, ensuring the robustness of this approach for targeted biosensing applications. Ultimately, our aim is to integrate this highly sensitive OCB design into a user-friendly, point-of-care testing device that can deliver rapid, reliable, and on-site analyses thereby expanding its practicality across diverse settings.

Data availability

The datasets generated during and/or analysed during the current study are available from the corresponding author on reasonable request.

Received: 8 November 2024; Accepted: 25 February 2025
Published online: 05 March 2025

References

1. Chen, C. & Wang, J. Optical biosensors: an exhaustive and comprehensive review. *Analyst* **145**, 1605–1628 (2020).
2. Rho, D., Breaux, C. & Kim, S. Label-free optical resonator-based biosensors. *Sensors* **20**, (2020).
3. Loyez, M., Adolphson, M., Liao, J. & Yang, L. From whispering gallery mode resonators to biochemical sensors. *ACS Sens.* **8**, 2440–2470 (2023).
4. Jiang, X., Qavi, A. J., Huang, S. H. & Yang, L. Whispering-gallery sensors. *Matter.* **3**, 371–392 (2020).
5. Tosi, D., Sypabekova, M., Bekmurzayeva, A., Molardi, C. & Dukenbayev, K. 6 - interferometers. In *Optical Fiber Biosensors* (eds. Tosi, D. et al.) 153–177 https://doi.org/10.1016/B978-0-12-819467-6.00006-8 (Academic Press, 2022).
6. Wang, R. et al. Label-free and selective cholesterol detection based on multilayer functional structure coated fiber fabry-perot interferometer probe. *Anal. Chim. Acta.* **1252**, 341051 (2023).
7. Ghasemi, M. et al. Fabry–Perot interferometric fiber-optic sensor for rapid and accurate Thrombus detection. *Biosens.* **13**, (2023).
8. Rho, D. & Kim, S. Demonstration of a label-free and low-cost optical cavity-based biosensor using streptavidin and C-reactive protein. *Biosens.* **11**, (2021).
9. Zhang, T., Gong, Z., Giorno, R. & Que, L. A nanostructured Fabry-Perot interferometer. *Opt. Express*. **18**, 20282–20288 (2010).
10. Tu, L., Huang, L. & Wang, W. A novel micromachined Fabry-Perot interferometer integrating nano-holes and dielectrophoresis for enhanced biochemical sensing. *Biosens. Bioelectron.* **127**, 19–24 (2019).
11. Toropov, N. et al. Review of biosensing with whispering-gallery mode lasers. *Light Sci. Appl.* **10**, 42 (2021).
12. Li, X. et al. A review of specialty fiber biosensors based on interferometer configuration. *J. Biophotonics*. **14**, e202100068 (2021).
13. Yu, D. et al. Whispering-gallery-mode sensors for biological and physical sensing. *Nat. Reviews Methods Primers*. **1**, 83 (2021).
14. Joy, C. & Kim, S. Benefits of a scaled differential calculation method for use in a Fabry-Perot based optical cavity biosensor. In *Texas Symposium on Wireless and Microwave Circuits and Systems (WMCS)* 1–4 https://doi.org/10.1109/WMCaS.2017.8070707 (2017).
15. Rho, D., Breaux, C. & Kim, S. Demonstration of a low-cost and portable optical cavity-based sensor through refractive index measurements. *Sensors* **19**, (2019).
16. Rho, D. & Kim, S. Low-cost optical cavity based sensor with a large dynamic range. *Opt. Express*. **25**, 11244–11253 (2017).
17. Rho, D. & Kim, S. Label-free real-time detection of biotinylated bovine serum albumin using a low-cost optical cavity-based biosensor. *Opt. Express*. **26**, 18982–18989 (2018).
18. Sypabekova, M., Hagemann, A., Kleiss, J., Morlan, C. & Kim, S. Optimizing an optical cavity-based biosensor for enhanced sensitivity. *IEEE Sens. J.* **23**, 25911–25918 (2023).
19. Wilchek, M. & Bayer, E. A. The avidin-biotin complex in bioanalytical applications. *Anal. Biochem.* **171**, 1–32 (1988).
20. Hermanson, G. T. Bioconjugate techniques: third edition. *Bioconjug. Techniques: Third Ed.* **1–1146** https://doi.org/10.1016/C2009-0-64240-9 (2013).
21. Sypabekova, M., Hagemann, A., Rho, D. & Kim, S. Review: 3-Aminopropyltriethoxysilane (APTES) deposition methods on oxide surfaces in solution and vapor phases for biosensing applications. *Biosens. (Basel)* **13**, (2023).

22. Gunda, N. S. K., Singh, M., Norman, L., Kaur, K. & Mitra, S. K. Optimization and characterization of biomolecule immobilization on silicon substrates using (3-aminopropyl)triethoxysilane (APTES) and glutaraldehyde linker. *Appl. Surf. Sci.* **305**, 522–530 (2014).
23. Zhu, M., Lerum, M. Z. & Chen, W. How to prepare reproducible, homogeneous, and hydrolytically stable aminosilane-derived layers on silica. *Langmuir* **28**, 416–423 (2012).
24. Cras, J. J., Rowe-Taitt, C. A., Nivens, D. A. & Ligler, F. S. Comparison of chemical cleaning methods of glass in preparation for silanization. *Biosens. Bioelectron.* **14**, 683–688 (1999).
25. Williams, E. H. et al. Immobilization of Streptavidin on 4H–SiC for biosensor development. *Appl. Surf. Sci.* **258**, 6056–6063 (2012).
26. Lee, G. U., Kidwell, D. A. & Colton, R. J. Sensing discrete Streptavidin-Biotin interactions with atomic force microscopy. *Langmuir* **10**, 354–357 (1994).

Author contributions
M.S: investigation, methodology, analysis, writing original draft. J.K: methodology A.H: methodology S.S: methodology R.W: methodology K.S: conceptualization of the idea, funding acquisition, supervision All authors reviewed the manuscript.

Funding
Research reported in this work was supported by NIGMS of the National Institutes of Health under award number R15GM146233.

Declarations

Competing interests
The authors declare no competing interests.

Additional information
Correspondence and requests for materials should be addressed to S.K.

Reprints and permissions information is available at www.nature.com/reprints.

Publisher's note Springer Nature remains neutral with regard to jurisdictional claims in published maps and institutional affiliations.